04-2103

JOURNAL OF NEUROTRAUMA
Volume 24, Number 3, 2007

Pp. 492–507
DOI: 10.1089/neu.2006.0149

Immediate Damage to the Blood-Spinal Cord Barrier due to Mechanical Trauma

JASON T. MAIKOS and DAVID I. SHREIBER

ABSTRACT

Primary damage to the blood–spinal cord barrier (BSCB) is a nearly universal consequence of spinal cord injury that contributes significantly to the overall pathology, including the introduction of reactive species that induce cytotoxicity as well as secondary insults on the BSCB itself. We have characterized quantitatively the extent and severity of primary, physical disruption of the BSCB in adult rats 5 min after graded trauma induced with the Impactor weight-drop model of spinal cord contusion. Animals were injured by dropping a 10-g mass 12.5, 25, or 50 mm ($n_{level} = 8$) on to the exposed mid-thoracic spinal cord. The volume of extravasation of three markers of distinct size—fluorescently labeled hydrazide (~730 Da), fluorescently labeled bovine serum albumin (~70 kDa), and immunohistochemically labeled red blood cells (~5 μm in diameter)—were quantified in both the gray and white matter. The results indicate that spinal cord trauma causes immediate, non-specific vascular changes that are well-predicted by mechanical parameters. Extravasation volume increased significantly with increasing drop height and decreasing marker size. Extravasation volumes for all three markers were greater in gray matter than in white matter, and were better correlated to the rate of spinal cord compression than to the depth of spinal cord compression, which suggests that tissue-level strain rate effects contribute to primary spinal cord microvasculature pathology. The relationship between the response of the spinal cord and the injury pattern points towards opportunities to control the distribution and extent of injury patterns in animal models of spinal cord injury through a precise understanding of model and tissue biomechanics, as well as potential improvements in means of preventing spinal cord injury.

Key words: biomechanics; blood–spinal cord barrier; hemorrhage; spinal cord injury

INTRODUCTION

New spinal cord injuries (SCI) occur in approximately 11,000 people each year in the United States (Berkowitz, 1998). Damage to the vasculature, notably the breakdown of the blood–spinal cord barrier (BSCB), is an almost universal consequence of SCI clinically as well as in animate models (Balentine, 1978; Faden et al., 1988; Noble et al., 1996). During SCI, the initial mechanical insult can disrupt the BSCB (primary injury), causing the non-specific influx of normally impermeable molecules and agents into the contused spinal cord. The blood-borne species that cross the compromised vasculature can range from small molecules (due to minor BSCB permeability changes) to red blood cells from gross hemorrhage (Dohrmann and Wick, 1971; Griffiths

Department of Biomedical Engineering, Rutgers, The State University of New Jersey, Piscataway, New Jersey.

and Miller, 1974; Beggs and Waggener, 1976; Faden et al., 1988; Noble and Wrathall, 1989a,b; Noble et al., 1996; Popovich et al., 1996). The mechanical disruption of the vasculature and BSCB then contributes to the evolution of secondary events that injure neighboring tissue, including continued insults on uncompromised sections of the BSCB that affect its function and lead to increased permeability, dictating a significant portion of the overall pathology following SCI (Mautes et al., 2000).

As such, the time course of vascular damage and BSCB breakdown has been studied extensively with several models of traumatic SCI, including weight-drop (Dohrmann et al., 1976; Noble and Wrathall, 1989a,b; Young, 2002), pneumatic/electromagnetic impactor (Bresnahan et al., 1987; Noyes, 1987; Stokes et al., 1992), and compression (Beggs and Waggener, 1975; Jaeger and Blight, 1997). A variety of techniques have been employed to evaluate BSCB injury, such as injection of probes (typically labeled albumin, labeled dextrans, or horseradish peroxidase) followed by qualitative or quantitative microscopy (Griffiths and Miller, 1974; Beggs and Waggener, 1975; Wagner and Stewart, 1981; Noble and Wrathall, 1987; Jaeger and Blight, 1997; Whetstone et al., 2003), radiolabeled tracers followed by autoradiography (Popovich et al., 1996), and contrast-enhanced magnetic resonance imaging (MRI) (Terae et al., 1997; Bilgen and Narayana, 2001). Most of these studies focus on BSCB permeability from hours to weeks post-injury, but a few examined acute changes (<5 min), where the bulk of injury can be assumed to be directly caused by overt vascular damage from primary mechanical perturbation of the tissue, rather than a combination of mechanics and secondary insults, which compromise BSCB function. Collectively, these studies indicate that initial permeability changes occur primarily in the gray matter and spread to the white matter during the first hours after injury, and can persist for as long as 1 month post-injury (Popovich et al., 1996). While these studies demonstrate that the degree of permeability changes increases with the severity of injury parameters (e.g., drop height for weight-drop injury), in no case has BSCB/microvascular integrity been correlated to the physical response of the tissue (e.g., compression distance and compression rate during weight drop). Moreover, while microvascular injury/BSCB permeability changes following SCI have been documented for a wide range of molecules—including [^{14}C]-α-aminoisobutyric acid (molecular weight [MW] = 103 Da), gadopentetate-dimeglumine (MW = 938 Da), horseradish peroxidase (MW $\approx$ 40 KDa), albumin (MW $\approx$ 70 KDa), a wide range of dextrans (MW $\approx$ 20,000–150,000), and red blood cells to indicate hemorrhage, it is difficult to draw quantitative conclusions regarding relative changes among these molecules because of the disparity of methods employed, and because, in most cases, changes were measured for only a single marker. A noted exception is Wagner and Stewart (1981), where extravasation of fluorescein-labeled dextrans, ranging from 20,000 to 150,000 in molecular weight (MW), was examined, each in separate animals, 8 h after injury, with no significant differences observed.

In the present study, acute changes to the BSCB due to mechanical disruption were quantified following experimental SCI in the rat using the Impactor weight-drop technique. The severity and extent of mechanically mediated BSCB injury were evaluated by determining the volume of molecule-, protein-, and cell-sized species that extravasated across injured vasculature into spinal cord parenchyma 5 min following trauma. Impact parameters (impact velocity, cord compression depth, and cord compression rate) measured during injury were correlated to the distribution of extravasation volume for a preliminary measure of BSCB sensitivity to specific mechanical variables, such as stress and strain.

METHODS

Surgical Procedure

Standard procedures for Multicenter Animal Spinal Cord Injury Study (MASCIS) Impactor experiments were followed (Young, 2002). Adult, female Long-Evans Hooded rats, 77 $\pm$ 5 days old (220–240 g; n = 33), were obtained from Simonsen Labs (Gilroy, CA) and housed for 1 week prior to experimentation to allow the rats to adapt to their environment. Following pentobarbital-induced anaesthesia (45 mg/kg, i.p), a T9-T10 laminectomy was performed under sterile conditions.

Blood-Borne Species Labeling Scheme

BSCB permeability was evaluated for three distinct species that spanned a wide range in size: Alexa Flour 568–labeled hydrazide (707 Da, 576-nm excitation, 599-nm emission; Molecular Probes, Eugene OR); Alexa Flour 488–labeled bovine serum albumin (BSA; ~70 kDa, 497-nm excitation, 520-nm emission; Molecular Probes); and native red blood cells (~5 μm in diameter). Ten minutes prior to injury, animals were given an intravenous injection into the femoral vein of 1 mL of tracer solution consisting of 1 mg/kg of the labeled hydrazide and labeled BSA dissolved in 0.9% saline.

Injury and Post-Injury Procedures

All contusions were performed using the MASCIS Impactor. The Impactor is a 10-g rod, with a 2.2-mm head. Rat spinal cords at age 77 days are approximately 3 mm

in width. Animals were suspended by clamping the T8 and T11 dorsal vertebral processes. The rod was centered over the laminectomy, raised to the appropriate height, and dropped onto the exposed dura. Impactor injury was performed at three drop heights ($n_{height} = 8$): 12.5, 25, and 50 mm. Additional animals ($n = 3$) received only the surgery, and one ($n = 1$) served as an unoperated control. Injury was produced 60 ± 2 min after anesthesia induction.

The Impactor rod is mechanically linked to a digital optical potentiometer (S2 Series; U.S. Digital, Vancouver, WA), which sends transitor-transitor logic (TTL; ±5 V) pulses for each small angular movement that allows the rod movements to be measured precisely at ±20 μm and ±20 μsec (Young, 2002). A micromanipulator is used to lower the Impactor head precisely on the surface of the spinal cord to determine the zero point. The rod is then raised to appropriate drop height and released for impact. The software detects rod release from change of rod position then collects a stream of TTL pulses from the digital potentiometers representing rod movements at a 20-kHz sampling rate. Contact with the spinal cord closes the circuit between the rod and the cord. The Impactor uses electrical contact to establish the time of contact, which allows the software to perform a linear regression of the rod movement 2 msec before contact with the spinal cord to estimate impact velocity (Young, 2002). A second probe is placed on the dorsal surface of the vertebral body immediately proximal to the laminectomy and is linked to a separate digital optical potentiometer to evaluate movement of the underlying spinal column. The depth of compression is then determined by subtracting the vertebral body motion from the motion of the impacting rod. Compression rate is estimated by dividing the compression distance by the duration from impact to reversal of the surface of the spinal cord. Impact velocity, cord compression distance, and cord compression rate were recorded for each experiment (Fig. 1).

At 5 min following injury, animals were euthanized with a lethal dose of pentobarbital (60 mg/kg), exsanguinated with 200 mL of heparinized saline, and perfused transcardially with 10% neutral buffered formalin. The spinal cords were removed and stored in 10% formalin until tissue processing. All procedures were approved by the Rutgers University Animal Care and Facilities Committee.

Tissue Preparation and Immunohistochemistry

Fixed spinal cords were sectioned horizontally into 20-μm sections with a cryostat (ThermoShandon, Pittsburgh, PA). Sections were mounted on charged glass slides (Superfrost Plus; Fisher, Pittsburgh, PA) in two serial sets.

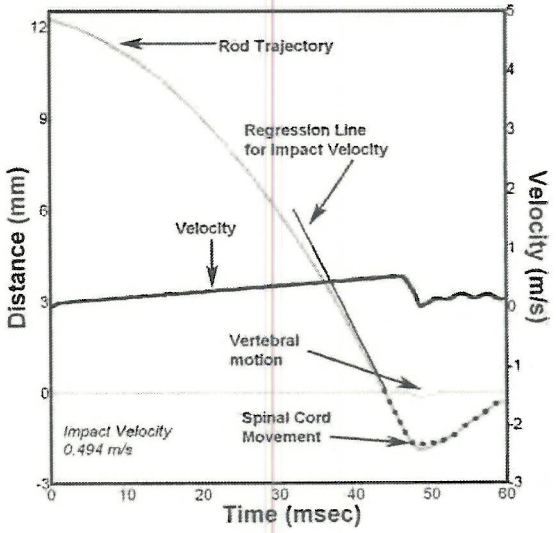

FIG. 1. Example output following Impactor weight-drop injury (12.5-mm drop height). Separate optical potentiometers record the motion of the impacting rod and the vertebral body adjacent to the impact site. Vertebral motion is subtracted from rod motion to arrive at the compression distance of the spinal cord. Vertebral motion contributed minimally to the total displacement of the spinal cord, and in this figure, the vertebral motion and resulting reduction in cord compression distance were scaled by a factor of 10 to assist in visualizing the displacement of the spinal column. The actual average motion was 0.059 ± 0.051 mm. The velocity is determined from the derivative of the rod trajectory position data, and velocity at impact is estimated by linearly regressing the position data 2 msec prior to impact. Spinal cord compression rate is found by dividing the compression depth by the time interval between impact and reversal of the surface of the spinal cord.

One set was immediately coverslipped (Prolong Antifade; Molecular Probes) and used for direct evaluation of extravasation of injected fluorophores. The other set was used to immunohistochemically label red blood cells using an immunostaining workstation (ThermoShandon). Slides were rinsed in wash buffer (phosphate buffered saline [PBS] + 1% bovine serum albumin [BSA] + 0.5% Triton) for 5 min at room temperature, and blocked for 1 h in 10% normal goat serum (NGS). Slides were incubated overnight at room temperature in a polyclonal rabbit anti-rat erythrocyte antibody (Research Diagnostics, Flanders, NJ; optimal dilution 1:100). Specificity of binding was confirmed in preliminary experiments by comparing to parallel sets of slices incubated in rabbit IgG antibody (Jackson ImmunoResearch, West Grove, PA), in which no immunoreactivity was observed. Slides were then washed for 5 min and incubated for 1 h in goat anti-rabbit Alexa Flour 647 (650-nm excitation, 668-nm emission; Molecular Probes). Slides were rinsed for 5 min and

coverslipped (Prolong Antifade; Molecular Probes) in preparation for epifluorescence imaging.

Quantifying Microvascular Pathology: Extravasation Volume Calculation

Horizontal sections were imaged with epifluorescent microscopy to detect fluorescently labeled hydrazide, albumin, and red blood cells. Approximately 40 sections were examined for each fluorophore for each spinal cord. In each section, separate mosaic images at each wavelength were generated using computer controlled microscopy (Olympus IX81; Olympus America, Center Valley, PA). It was possible to identify general areas of uninjured gray and white matter in each section by visually comparing the section to parallel sections from unoperated controls. These areas were generally at the proximal and/or distal extremes of the section, which were the farthest away from the impact site. In some sections, the gray/white matter border was masked by the extravasated fluorophore(s) or immunolabeled cells. In these cases, the borders were estimated by extending regions that were visible and again comparing to parallel sections from unoperated, unlabeled control tissue. Representative areas of uninjured gray and white matter were then selected in each section, and the maximum pixel grayscale values in those areas were identified and used to threshold that section. Any grayscale pixel value above the highest "uninjured" pixel value was considered injured. From the binary images, the areas of extravasation for both gray matter and white matter were calculated for each section, summed across sections, and multiplied by the linear distance between images to arrive at separate "extravasation volumes" for each fluorophore for gray and white matter. These gray and white matter volumes were then summed to arrive at a total extravasation volume for each fluorophore for each spinal cord.

Statistical Analysis

The effects of drop height and fluorescent marker on extravasation volume were determined statistically with separate one-way analyses of variance (ANOVAs)—$p < 0.05$. Additionally, injury volume measurements were linearly regressed against tissue compression rate, compression distance, and impact velocity measured experimentally to confirm any correlations.

RESULTS

Extravasation Morphology

The patterns of extravasation were similar for all three markers, and generally matched previously reported observations (Noble and Wrathall, 1989) (Figs. 2–4). In horizontal sections, areas demonstrating extravasation were roughly oblong in shape, with the major axis aligned axially with the spinal cord. Extravasation was more pronounced and extended further in the rostral and caudal directions in the highly vascular gray matter versus white matter. Areas of extravasation in a given tissue slice were visibly larger as drop height increased and as the size of the labeled marker decreased.

Extravasation Volume

The volume of extravasation of each fluorescently labeled marker was quantified using image analysis by generating a binary image with the average grayscale pixel value of uninjured tissue in both gray and white matter as the thresholds. Extravasation volume increased significantly with increasing drop height (ANOVA, $p < 0.001$; Fig. 5) and with decreasing marker size (ANOVA, $p < 0.001$; Fig. 6). Post hoc, pairwise comparisons revealed significant differences between each pair of drop heights ($p < 0.001$) and each pair of markers ($p < 0.031$; Scheffe's test). Additionally, extravasation volumes were significantly greater in gray matter vs. white matter, and each significantly contributed to the total extravasation volume (ANOVA, followed by Scheffe's test, $p < 0.001$). No extravasation of the labeled hydrazide, albumin, or erythrocytes was observed in either surgical shams or the unoperated control.

Correlations to Impact Parameters

Average impact parameters (impact velocity, cord compression depth, and cord compression rate) for each loading condition are summarized in Table 1. Vertebral motion, which was subtracted from the displacement of the rod to arrive at the cord compression distance, contributed minimally to the overall displacement of the cord (average vertebral displacement = 0.059 ± 0.051 mm), and no consistent trends were observed relating the vertebral motion to drop height (ANOVA, $p = 0.078$). The results of linear correlations of gray and white matter extravasation volumes to the physical impact parameters measured during Impactor weight-drop injury are summarized in Table 2. Impact velocity (Fig. 7), cord compression distance (Fig. 8), and cord compression rate (Fig. 9) were highly correlated to extravasation volume for each marker (minimum $R^2 = 0.735$), although the coefficients were generally greater for impact velocity and compression rate than for compression distance. In many cases, the y-intercept of the correlation was negative, which implies a positive x-intercept, because of the positive slope for all lines. A positive value of the x-intercept indicates the minimum magnitude of the particular

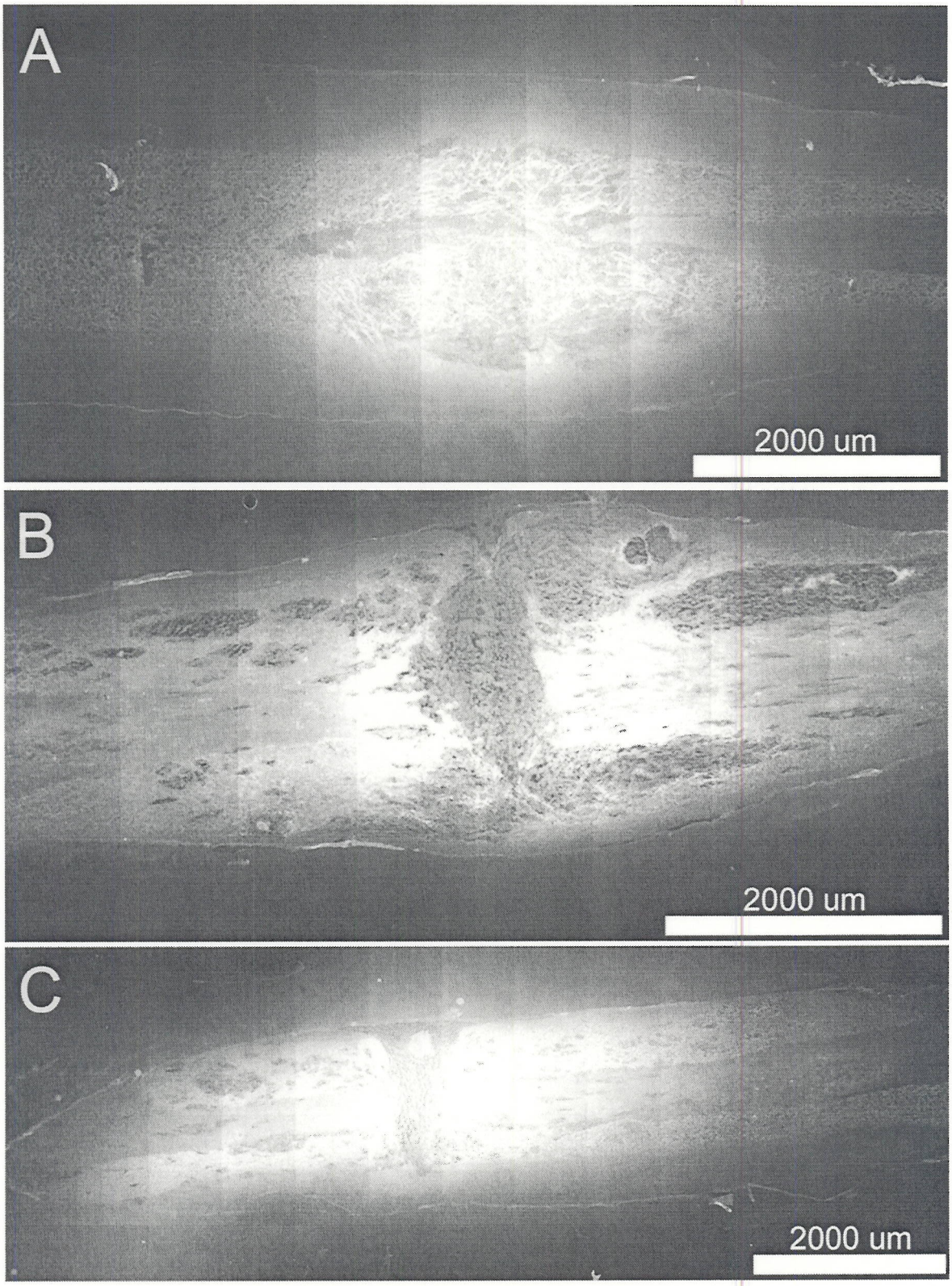

FIG. 2. Representative images of immediate hydrazide extravasation for 12.5 mm (**A**), 25 mm (**B**), and 50 mm (**C**) drop heights. The area of hydrazide extravasation increased as drop height increased. Damage is observed in both the gray and white matter.

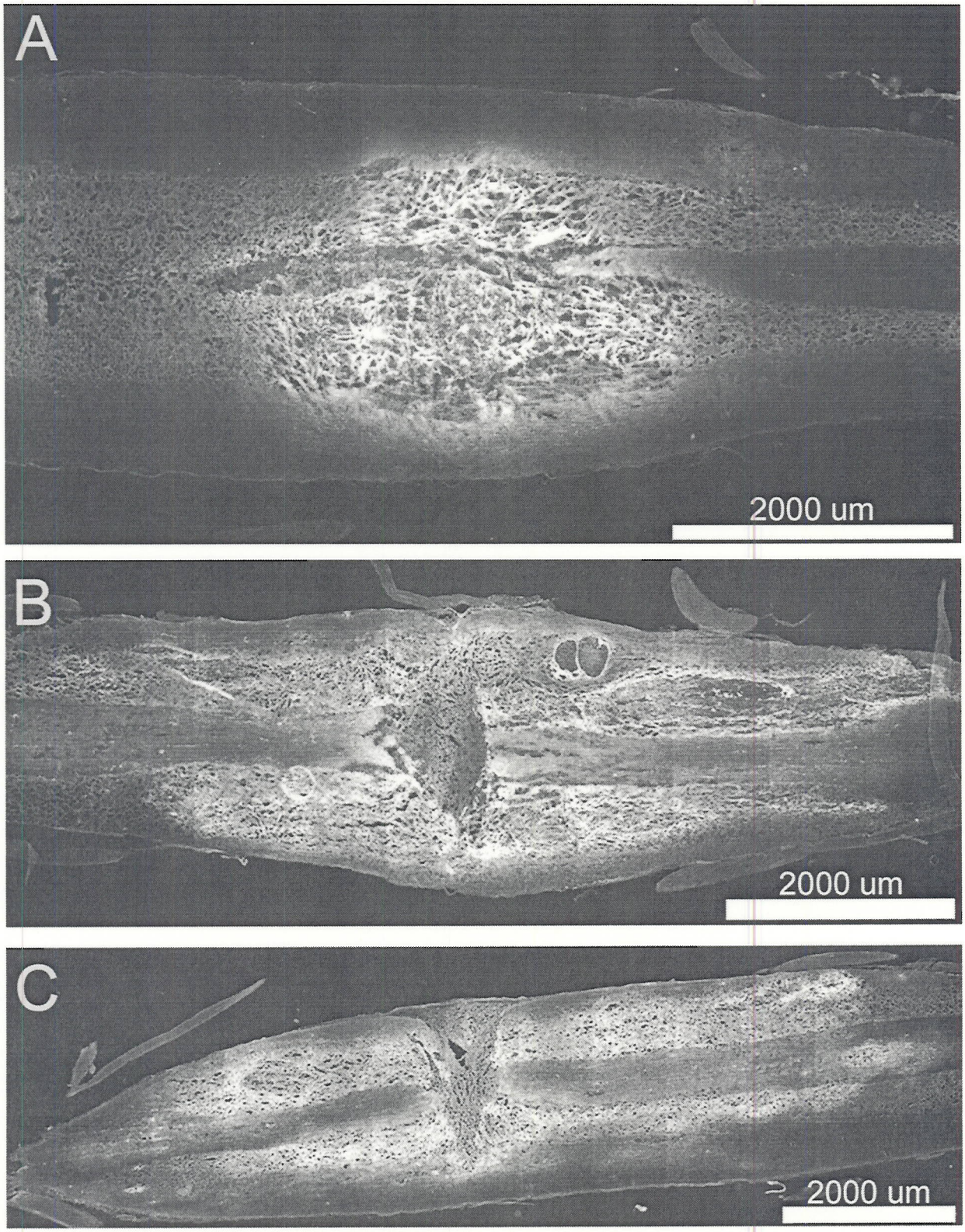

FIG. 3. Representative images of immediate albumin extravasation for 12.5 mm (**A**), 25 mm (**B**), and 50 mm (**C**) drop heights. The area of albumin extravasation increased as drop height increased. Damage is observed in both the gray and white matter. The sections shown depict increased BSCB damage in the dorsal horns of the gray matter versus central white matter.

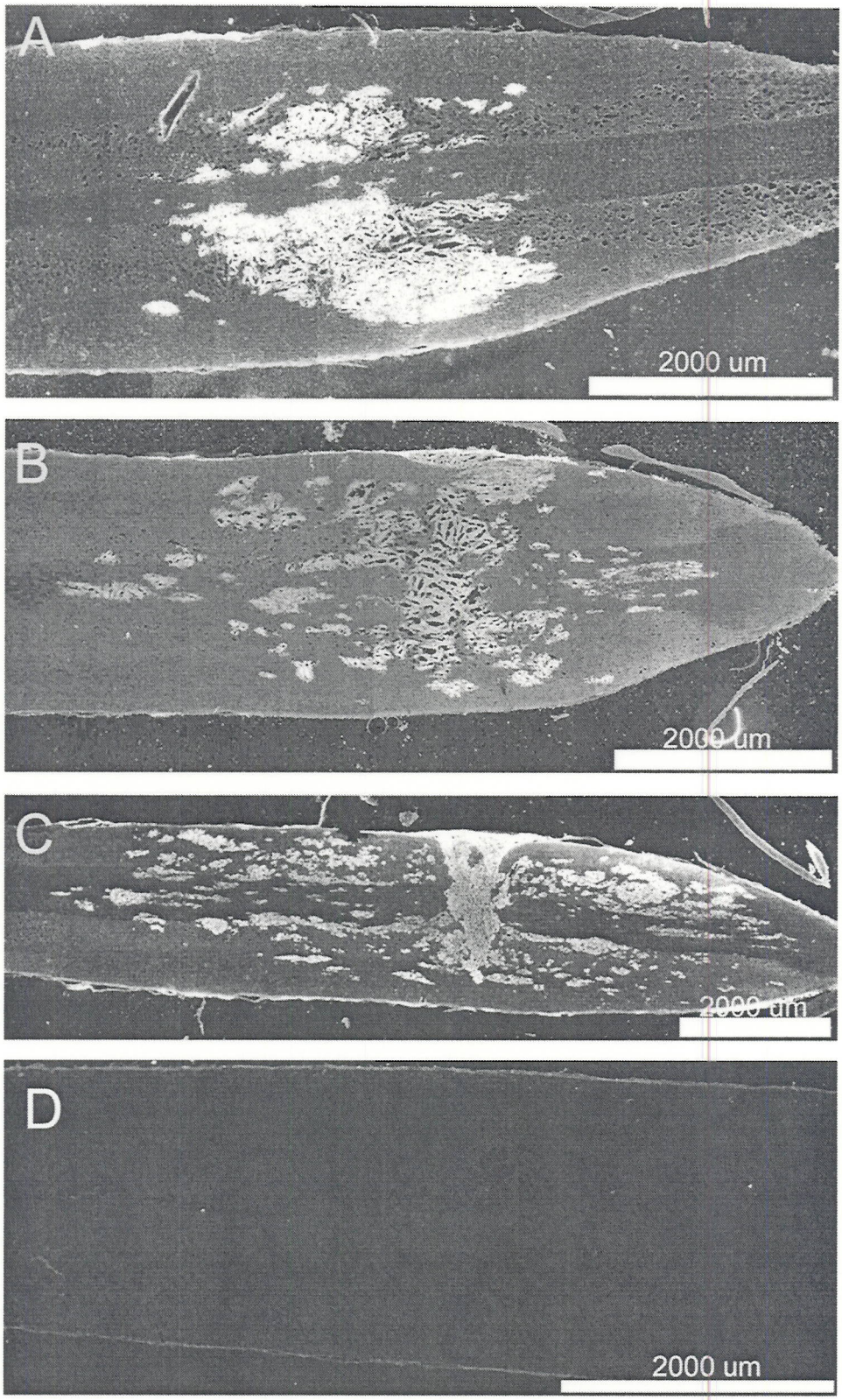

FIG. 4. Representative images of microvascular hemorrhage as indicated by immunolabeling of red blood cells for 12.5 mm (**A**), 25 mm (**B**), and 50 mm (**C**) drop heights. The area of RBC extravasation increased as drop height increased. Damage is observed in both the gray and white matter. Immunolabeling with a rabbit IgG control demonstrated minimal non-specific labeling (**D**).

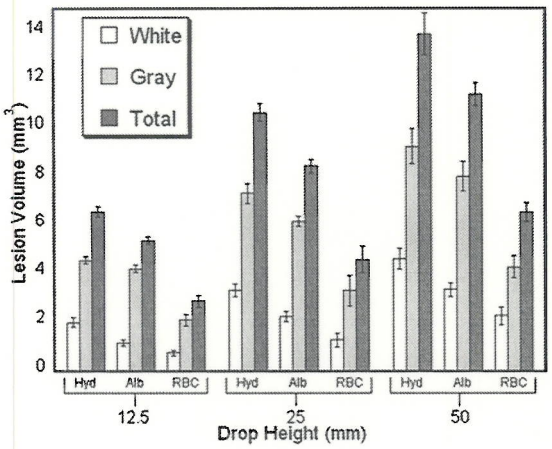

FIG. 5. Extravasation volumes of the three species as functions of drop height. Extravasation volumes differed significantly with drop height and with injury marker (ANOVA, $p < 0.001$). Injury to the gray matter was significantly greater than injury to the white matter, and each contributed significantly to the overall, total extravasation volume (ANOVA, $p < 0.001$). Post-hoc pairwise comparisons revealed significant increases for each drop height combination for both gray and white matter (Scheffe's post hoc test, $p < 0.01$).

impact parameter required to produce non-zero extravasation, and can be viewed as a threshold for injury. However, the 95% confidence intervals for the y-intercept for all of the correlations of extravasation volumes in gray matter to impact parameters encompass zero; the "thresholds" cannot, therefore, be distinguished from zero, and any compression will be predicted to produce injury to gray matter. For the white matter, only one correlation (hydrazide vs. compression depth) yielded confidence intervals on the y-intercept that encompassed zero. Inverse correlations of the remaining white matter extravasation volumes to impact parameters (injury volumes as the independent variables, impact parameters as the dependent variables) showed increasing thresholds for larger species than smaller ones. Collectively, the results indicate that microvasculature in the gray matter is more sensitive to compressive loads than that in the white matter, and that above certain thresholds for tissue compression and rate of tissue compression, the microvasculature of the white matter can be injured. Table 2 also includes correlation coefficients relating drop height to velocity^2 (which should be related by $2\times$ the gravitational constant) and velocity to cord compression rate, both of which are often used to evaluate the quality and reproducibility of Impactor experiments.

DISCUSSION

We have chosen to focus on characterizing the immediate breakdown of the microvasculature due to trauma because of the dramatic effects microvascular damage has

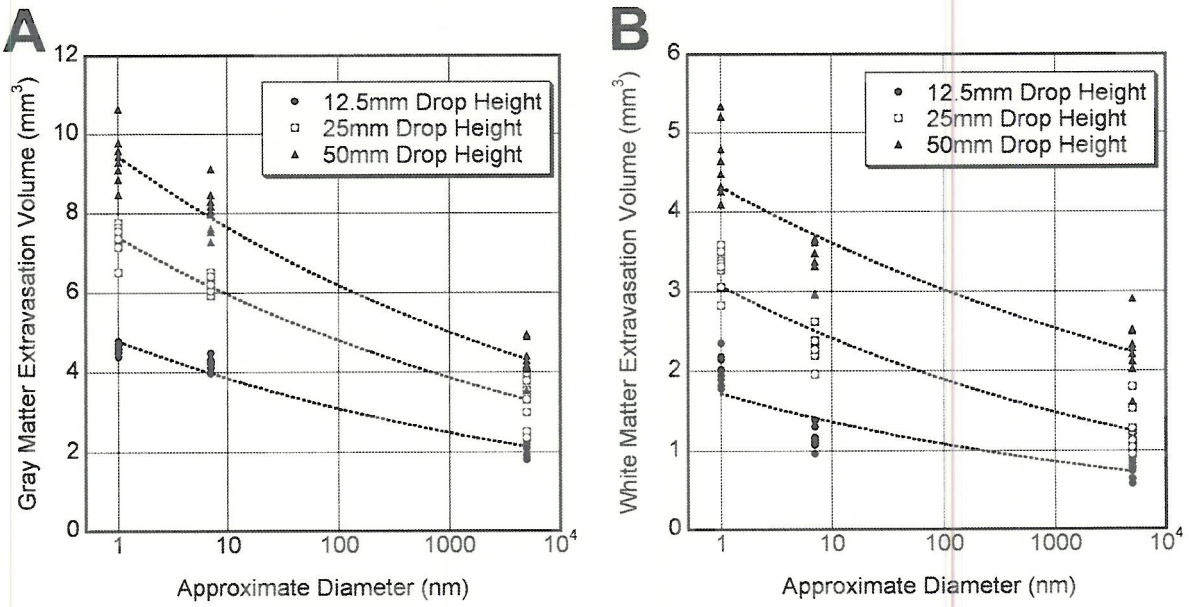

FIG. 6. Consistent relationships were observed between extravasation volume and blood-borne marker diameter (Alexa 568 Hydrazide, ~1 nm; Alexa 488 Albumin, ~7 nm; red blood cells, ~5 μm) for both the gray matter (**A**) and the white matter (**B**) among the three drop heights. The extravasation volume in each tissue significantly depended on the marker size (ANOVA, $p < 0.001$). Pairwise post-hoc analysis (Scheffe's test) identified significant differences between each pair of markers ($p < 0.05$).

TABLE 1. SUMMARY OF IMPACT PARAMETERS AND LESION VOLUMES

Drop height (mm)	n	Velocity (mm/msec)	Compression depth (mm)	Compression rate (mm/msec)	Extravasation volume (mm^3)					
					Hydrazide		Albumin		Red blood cells	
					Gray	White	Gray	White	Gray	White
12.5	8	0.489	1.65	0.429	4.57	2.02	4.23	1.16	2.12	0.770
		(0.011)	(0.194)	(0.145)	(0.150)	(0.195)	(0.146)	(0.132)	(0.238)	(0.110)
25	8	0.690	2.14	0.586	7.36	3.32	6.21	2.27	3.32	1.29
		(0.007)	(0.168)	(0.023)	(0.411)	(0.260)	(0.212)	(0.224)	(0.620)	(0.273)
50	8	0.974	2.88	0.828	9.30	4.64	8.07	3.38	4.30	2.28
		(0.012)	(0.157)	(0.032)	(0.727)	(0.447)	(0.589)	(0.285)	(0.458)	(0.383)

Results are average (STD deviation).

on the secondary events and neuropathology following SCI. Secondary injury is an evolution of events—including inflammation, ischemia, and oxidative damage, as well as other factors, such as toxic amounts of nitric oxide (NO) production—that injure otherwise unaffected spinal cord tissue (Mautes et al., 2000). These secondary effects are the principal targets of post-trauma therapy and, as such, have been researched extensively in labo-

TABLE 2. SUMMARY OF LINEAR CORRELATIONS BETWEEN IMPACT PARAMETERS AND LESION VOLUMES

X	Y		Slope (+/− 95% conf. limits)	Intercept (+/− 95% conf. limits)	R^2	Predicted threshold
Velocity (mm/ms)	Hydrazide (mm^3)	Gray	9.51 (8.13, 10.9)	0.259 (−0.766, 1.28)	0.899	—
		White	5.37 (4.71, 6.05)	−0.530 (−1.03, −0.03)	0.923	0.069
	Albumin (mm^3)	Gray	7.78 (6.86, 8.71)	0.584 (−0.105, 1.27)	0.930	—
		White	4.54 (4.09, 5.00)	−0.992 (−1.33, −0.650)	0.948	0.191
	Red blood cell (mm^3)	Gray	4.42 (3.41, 5.43)	0.074 (−0.680, 0.829)	0.779	—
		White	3.11 (2.49, 3.73)	−0.787 (−1.25, −0.326)	0.824	0.246
Compression depth (mm)	Hydrazide (mm^3)	Gray	3.28 (2.47, 4.10)	−0.232 (−2.09, 1.63)	0.750	—
		White	1.86 (1.42, 2.29)	−0.805 (−1.81, 0.195)	0.769	—
	Albumin (mm^3)	Gray	2.78 (2.24, 3.32)	−0.017 (−1.25, 1.21)	0.832	—
		White	1.61 (1.29, 1.92)	−1.31 (−2.02, −0.591)	0.830	0.794
	Red blood cell (mm^3)	Gray	1.62 (1.20, 2.04)	−0.359 (−1.31, 0.596)	0.735	—
		White	1.14 (0.878, 1.40)	−1.09 (−1.69, −0.492)	0.778	0.973
Compression rate (mm/ms)	Hydrazide (mm^3)	Gray	11.1 (9.17, 13.1)	0.229 (−1.0, 1.49)	0.855	—
		White	6.51 (5.79, 7.23)	−0.673 (−1.13, −0.214)	0.938	0.134
	Albumin (mm^3)	Gray	9.17 (7.79, 10.5)	0.535 (−0.339, 1.41)	0.892	—
		White	5.45 (4.88, 6.02)	−1.08 (−1.44, −0.716)	0.945	0.220
	Red blood cell (mm^3)	Gray	5.21 (3.91, 6.51)	0.046 (−0.782, 0.874)	0.747	—
		White	3.69 (2.89, 4.48)	−0.819 (−1.32, −0.315)	0.800	0.297
*Drop height (mm)	Velocity^2 (mm^2/ms^2)		0.019 (0.0185, 0.0193)	0.002 (−0.011, 0.016)	0.997	N/A
**Velocity (mm/ms)	Compression rate (mm/ms)		0.826 (0.778, 0.872)	0.022 (−0.016, 0.057)	0.983	N/A

For correlations where the bounds of the confidence interval on the y-intercept did not encompass zero, the inverse correlation was performed, and a prediction of the threshold was identified from the lower bound of the y-intercept of the inverse correlation. When the bounds encompassed zero, it was assumed that the intercept could not be distinguished from zero, and therefore any positive perturbation would be predicted to cause injury.

*Assuming a gravitational acceleration constant of 9.8 m/s^2, the theoretical slope of the (Velocity^2 vs. Drop Height) line should be 0.0196 mm/ms^2. The 3% error observed is due to frictional losses.

**The correlation coefficient (R^2) between Compression Rate and Velocity is used as a measure of the quality of Impactor experiments and experimenter proficiency. Values above 0.9 are generally considered acceptable.

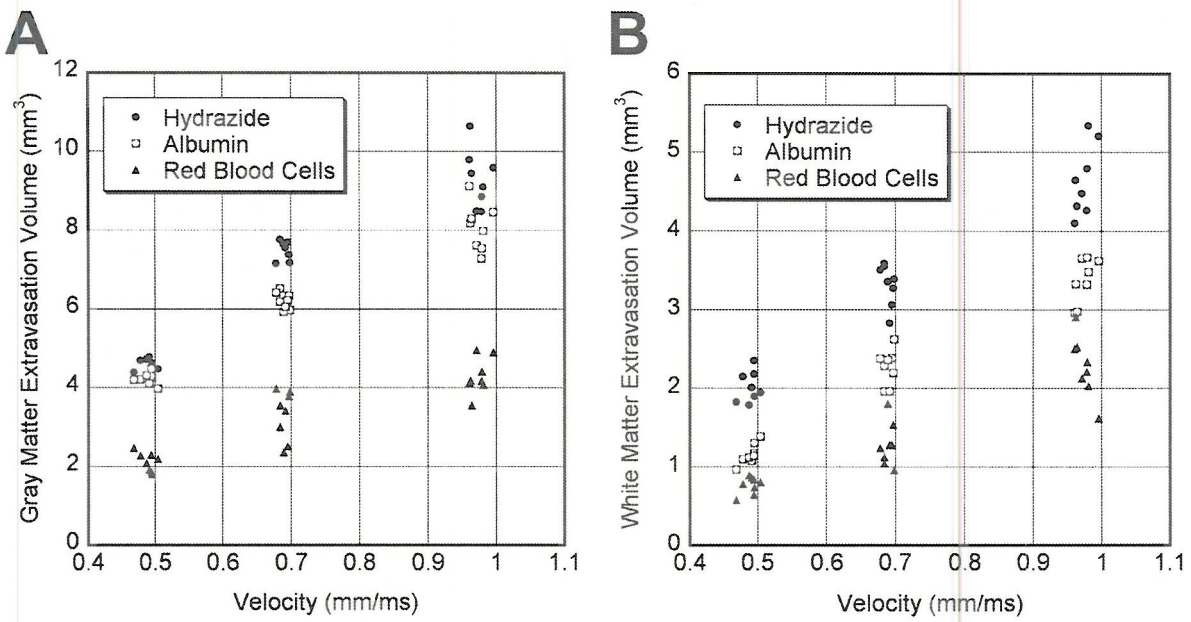

FIG. 7. Gray matter (**A**) and white matter (**B**) extravasation volumes of the three species as a function of impact velocity. Linear correlations of injury volumes to velocity indicated that gray matter was more sensitive to changes in impact velocity than white matter (minimum $R^2 = 0.779$; summarized in Table 2).

ratory and clinical settings (Blight, 1992; Popovich et al., 1997; Amar and Levy, 1999). By identifying the early breakdown of the spinal cord microvasculature via primary, mechanical damage to the BSCB, we can provide strategies for SCI therapies or prevention to limit the effect of the secondary sequelae.

Herein, we have presented a simple means of characterizing the severity and extent of damage to the BSCB in the spinal cord gray and white matter following SCI. Severity and extent are often difficult to distinguish in any model of CNS trauma. In many cases, a binary measure of injury is used that indicates the presence or absence of damage (for instance, cell death), from which an appraisal of the severity is inferred. Charting the causal factors that dictate the severity and extent of injury becomes increasingly difficult with time, as secondary insults add to the picture. The BSCB offers a convenient structure to examine both the severity and extent of tissue damage, in that the spatial permeability to different sized species can be easily examined in the same animal following spinal cord trauma. Thus, the extent of injury can be assessed by examining the extravasation volume of a particular marker, and the severity can be assessed by comparing extravasation volumes among marker sizes.

To our knowledge, this represents the first attempt to discriminate size-dependent microvascular changes quantitatively in the same animal in a clinically relevant trauma model. Wagner and Stewart (1981) qualitatively examined the extravasation of a series of fluorescently labeled dextrans and albumin eight hours following weight-drop injury in the cat, and the markers were studied in separate animals. Though the distance of migration from the injury epicenter was reported to be similar, it is difficult to compare to the results of this study because of the lack of quantitation, and because the extended survival time permits extravasation from secondary insults on the BSCB, as well as significant diffusion of the markers during the 8 h of circulation. Pan and colleagues have characterized temporal changes in the extent of BSCB permeability to sucrose, albumin, and tumor necrosis factor–α (TNF-α) following transection (Pan et al., 1997) or hemisection (Pan et al., 2003) in the mouse, and found non-specific immediate permeability changes at the injury site consistent with mechanical injury, but also subsequent species-specific variations that potentially depended on the specific cellular mechanisms that govern crossing of that molecule as well as the secondary insults. Thus, evaluating these changes for different degrees of mechanical insults acutely after injury, before significant secondary insults can manifest, allows improved correlation of extent and severity to the primary, mechanical parameters.

The trends relating BSCB damage to the physical parameters of Impactor weight-drop SCI are consistent with previous measures of the volume of cell death, open field

locomotor test scores (e.g., Basso, Beattie, Bresnahan Score [BBB]), and white matter sparing (Young 2002). Not surprisingly, for all measures, the degree of injury significantly increases as the drop height is increased. In this study, both the severity and extent of injury increased with drop height and was greater in the gray matter than the white matter, though immediate, mechanically mediated damage to the microvasculature of the white matter was observed. Correlation of the physical parameters measured during injury to the extravasation volumes allows a preliminary assessment of the sensitivity of the BSCB to specific mechanical variables. As with previous studies of lesion volume, BBB score, and white matter sparing, the extravasation volumes of each of the three species were better correlated (linearly) to impact velocity and compression rate than compression depth, though regression coefficients for all were statistically significant ($p < 0.001$) (Noble and Wrathall, 1987, 1989; Fehlings and Tator, 1995; Basso et al., 1996; Young, 2002). For all measures, the slopes of the linear correlations indicated that the gray matter was more sensitive to the impact parameters than the white matter. It is known that the mechanical properties of gray and white matter are different (Bilston et al., 2001; Arbogast and Margulies, 1998; Prange and Margulies, 2002), which will alter tissue movement and deformation spatially and temporally following impact. Additionally, the gray matter is more vascularized with a denser and more isotropically oriented microvascular network than the white matter. Thus, the sensitivity of the microvasculature to injury may be affected by inherent physical differences in the microvessels, such as vessel caliber or constituent cells comprising the BSCB, and the distribution of stress and strain through the tissue, which is influenced at the microscopic and mesoscopic scales by the vascular network and other structural components of the spinal cord, such as axons and other glia.

Mechanical thresholds for injury, predicted from inverse correlations when the confidence intervals on the y-intercept did not span zero, indicated that the white matter could generally tolerate some compression before demonstrating a compromised BSCB. In no cases could the thresholds for gray matter injury be distinguished from zero. These thresholds are more specific to the weight-drop injury technique and are difficult to generalize to other models or clinical situations, because the geometry and boundary conditions of the Impactor are not considered. An improved prediction would be based on the tissue-level material response (e.g., tissue stress and/or strain), which could be predicted by a computational analysis of tissue biomechanics and then generalized to other models and situations.

Interestingly, the slopes of the linear correlations between compression rate and lesion volume were greater than those between impact velocity and lesion volume for each of the three species, indicating the sensitivity of lesion volume to the rate of tissue displacement. Together, these suggest that the BSCB is sensitive to both mechanical strain and strain rate, indicating that the injury tolerance of the tissue depends on its viscoelastic properties. However, the only way to conclusively demonstrate the effect of strain rate on BSCB injury is to hold compression depth constant and vary compression rate or to vary compression depth and hold compression rate constant, which can be done with other pneumatic or electromagnetic impact devices (Stokes et al., 1992) or by placing a mechanical stop that limits Impactor displacement and therefore the cord compression depth.

To evaluate the severity of BSCB damage, the size-dependent permeability of the BSCB following injury was examined. Three markers were chosen that spanned a wide range of sizes: Alexa 568 hydrazide, which is a 707-Da non-toxic, fluorescently labeled ion most often used as a neuronal tracer; Alexa 488-labeled BSA, which has a molecular weight of approximately 70 kDa; and red blood cells, which have a nominal diameter of ~ 5 μm. The fluorescent hydrazide can be fixed in cells and tissues with common aldehyde-based fixatives. BSA has been routinely used as a marker of blood–brain barrier and BSCB injury, typically by labeling with Evans Blue (Griffiths and Miller, 1974; Wagner and Stewart, 1981; Noble and Maxwell, 1983). The hydrazide and BSA extravasation were visualized directly in the same tissue section. The red blood cells, a marker of hemorrhage, were indirectly visualized with immunohistochemistry in alternate sections. The initial hope was to examine all three markers in the same section to streamline post-processing and imaging, and provide an identical section for snapshots of injury severity. However, the fluorescence from the hydrazide weakened significantly during the immunohistochemical procedure, which prompted evaluating the directly labeled and indirectly labeled markers in different sections. It would be possible to circulate a red blood cell–specific labeled antibody, or to remove red blood cells, label them, and return them to circulation, to examine all markers in one section. The area of extravasation for a given species only changed gradually from section-to-section (20 μm apart), indicating that the different markers could be compared fairly in adjacent sections.

We selected the hydrazide and albumin based on their molecular weight, but a better measure would be the geometric size of the molecule or protein, since the species are generally excluded by size. Injury of greater severity will generate bigger holes in the vasculature to allow

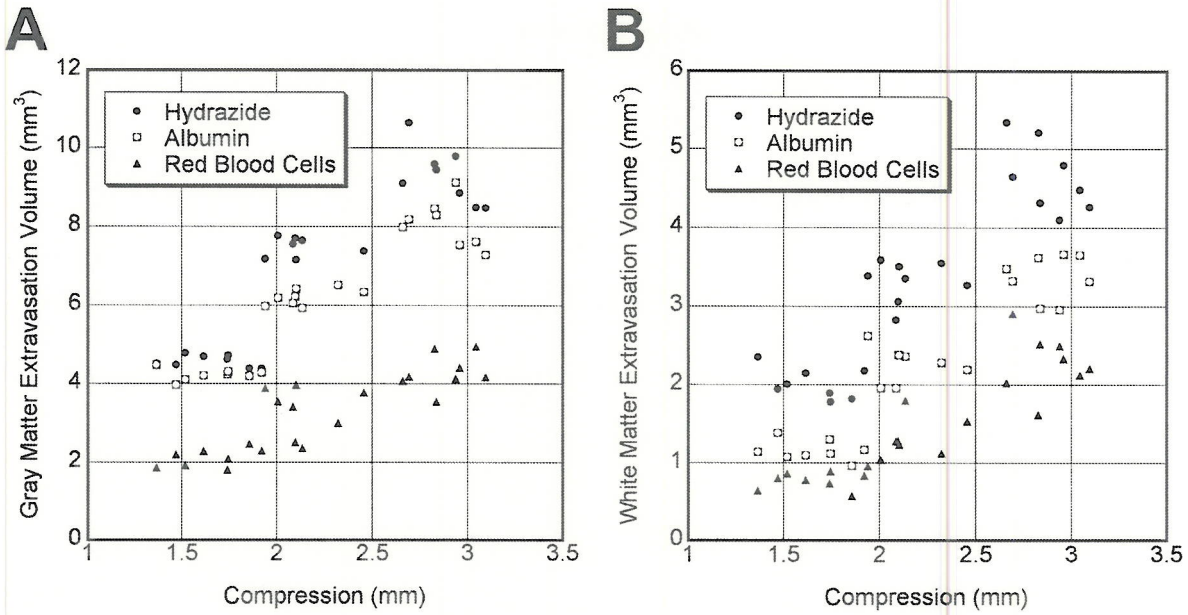

FIG. 8. Gray matter (**A**) and white matter (**B**) extravasation volumes of the three species as a function of cord compression distance. Compression distance is related to the magnitude of mechanical strain experienced by the tissue. Extravasation volumes were linearly correlated to compression (minimum $R^2 = 0.735$; summarized in Table 2). Gray matter was more sensitive than white matter to changes in compression depth.

larger species area-wise to extravasate into the parenchyma. The subsequent diffusion of these species through the parenchyma will also be dictated by their size. Whereas an effective diameter for red blood cells can be directly measured, the size of proteins and smaller molecules is typically determined from x-ray crystallography studies and/or molecular dynamics simulations. An estimate of the diameter of albumin (~7 nm) was taken

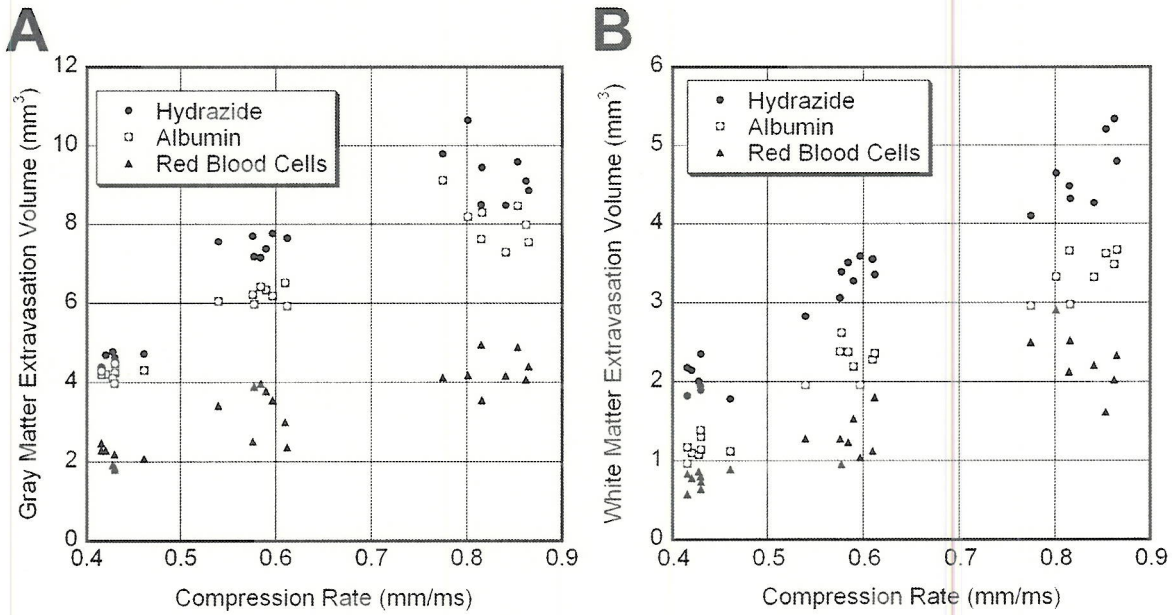

FIG. 9. Gray matter (**A**) and white matter (**B**) extravasation volumes of the three species as a function of cord compression rate. Compression rate is related to the magnitude of strain rate experienced by the tissue during trauma. Extravasation volumes were linearly correlated to compression rate (minimum $R^2 = 0.747$; summarized in Table 2). As with the other measures, gray matter was more sensitive than white matter to changes in compression rate.

from such studies by Sugio et al. (1999). However, no studies on the size of the labeled hydrazide were found. The diameter of a fluorescently labeled hydrazide ion, based on its molecular weight and specific gravity (1.032), was approximated at ~1 nm, which is on the same order as that experimentally measured for similarly sized tracers, such as Lucifer yellow (Stewart, 1981). Extravasation volume is plotted versus the approximate diameter of the three species in Figure 6. The three sets of data, one for each drop height, depict similar, semi-logarithmic trends. For all three species, no extravasation was observed in control tissue, demonstrating that the selective transport across the BSCB by specific mechanisms is negligible. For an improved prediction of size-dependent permeability, other markers could be included at different molecular weights/effective diameters, such as lysine-fixable fluorescent dextrans, or labeled immunoglobulins. Calibrated microspheres and nanoparticles could also be employed.

These sizes were generally selected to span blood-borne elements that may contribute to the secondary insults. Most obviously, increasing the protein content of the extracellular space induces vasogenic edema (Beggs and Waggener, 1975). Certain blood-borne molecules may have more specific effects following SCI. For example, quinolinic acid, a small neurotoxic molecule (~170 Da), causes overstimulation of neuronal cells, and serum-derived quinolinic acid that crosses the BSCB following trauma has been suggested to contribute significantly to cytotoxicity and secondary insults (Popovich et al., 1994). Endothelin-1 (ET-1), a 21–amino acid peptide, has been shown to cause an increase in BSCB disruption (Mautes et al., 2000). As a vasoconstrictor, ET-1 can cause ischemia in the spinal cord, resulting in increased cell death (McKenzie et al., 1995; Westmark et al., 1995). Serum contains high concentrations of complement, which ranges in size from ~80 to 200 kD (Anderson et al., 2004). Activation of several complement pathways has been demonstrated following spinal cord injury *in vivo*, and contributes to the demyelination and neurodegeneration in numerous pathological CNS conditions, including traumatic brain injury (Anderson et al., 2004). Neutrophils (8–15 μm) have been shown to amplify vascular injury by amassing at sites of vascular injury and secreting supplementary free oxygen radicals, furthering the vascular damage (Hernandez et al., 1987). Since secondary insults to the BSCB may not produce non-specific breakdown, but rather distinct permeability changes to different molecules, identifying the scope of primary, mechanically mediated BSCB injury takes on enhanced importance in potentially predicting the pattern of secondary insults based on the location of non-specifically extravasated, blood-borne species. It also provides a template for potential acute delivery of neuroprotective molecules.

One long-term aim for this research is to link the patterns of BSCB primary injury, and ultimately other primary pathologies, to the tissue-level states of mechanical stress and strain. Herein, we have correlated the distribution of BSCB injury of varying severity to the physical parameters associated with the Impactor (impact velocity, compression depth, and compression rate), as can be done with other impact trauma models of SCI. Each model has unique features, such that, for instance, BSCB injury following trauma induced to the same compression depth with direct weight-drop models, weight-drop models with "impact buttons," and controlled pneumatic or electromagnetic impactors can result in significantly different results, because of differences in the external loading conditions. However, the relationship between primary injury patterns in these models (and, in fact, any traumatic SCI) and the "internal," tissue-level stress and/or strain will be the same. We hope to determine this relationship by simulating the biomechanics of the weight drop model with finite element techniques, and quantitatively comparing the results of the finite element model to the spatial profiles of immediate BSCB permeability changes to predict threshold levels of stress and strain responsible for a given injury severity. These thresholds represent tissue-level targets for preventing SCI. Moreover, similarly modeling the mechanics of other models computationally will allow improved comparisons of results from laboratory to laboratory based on the internal, tissue-level criteria, and ultimately to improved standardization of injury patterns.

Understanding the sensitivity of the BSCB to mechanical perturbations potentially has important implications in targeted drug and gene delivery to the spinal cord. While methylprednisolone—the most effective drug to date clinically (Baptiste and Fehlings, 2006)—is a steroid that will naturally cross the BSCB—other promising therapies include peptide growth factors, antibodies, and/or proteins, which are generally larger than molecules that pass non-specifically through the barrier (<500 Da). In many cases, it is assumed that the compromised BSCB offers no resistance to therapies delivered via the circulatory system (Sharma, 2005). Clearly, following clinically relevant trauma, the BSCB is almost universally compromised to a graded extent and severity, and different sized blood-borne species will differentially cross into the parenchyma. Thus, therapies delivered to the spinal cord via the bloodstream (either directly or absorbed) will be naturally delivered to specific regions according to the severity of BSCB injury at the particular locations, and certain areas may not receive sufficient doses of the therapy (Sharma, 2005).

Understanding the size-specific severity of trauma to the BSCB can also be critical in determining a course of therapies to ameliorate the damage. For instance, statins have recently been shown to reduce CNS inflammation following SCI (Stanislaus et al., 2001; Pannu et al., 2005). Stanislaus and colleagues reported that, after induction of experimental allergic encephalomyelitis (EAE: the animal disease for multiple sclerosis) in rats, Lovastatin helped stabilize the BSCB by decreasing mononuclear cells penetration into the spinal cord, as well as obstructing the expression of inducible nitric oxide synthase (iNOS) and proinflammatory cytokines (Stanislaus et al., 1999, 2001). Mooradian et al. (2005) demonstrated that statins improved BBB function in a rat model of diabetes, limiting permeability of species as small as 40 kD (the smallest tested). Different statin formulations maintain different abilities to cross the blood–brain/blood–spinal cord barrier according to their lipophilicity, and there is evidence that, in some cases, indiscriminant crossing of statins into brain and spinal cord parenchyma causes significant CNS side effects and is deleterious to long-term viability (Botti et al., 1991; Guillot et al., 1993; Kostis et al., 1994; Quion and Jones, 1994; Sparks et al., 2002). Other promising acute therapies include antibodies targeted against immune-modulators such as FAS (CD95) (Demjen et al., 2004), which is a member of the TNF-α receptor family, and CD11d, which regulates leukocyte adhesion (Saville et al., 2004; Bao et al., 2005). As such, combination therapies could be designed that provide one measure for mildly injured areas (for instance, atorvastatins to begin to seal the BSCB), and another measure for severely injured ones (for instance, potent mediators of inflammatory cell adhesion). Poly(ethylene glycol) (PEG) has also been shown to assist in sealing damaged axonal membranes (Borgens and Shi, 2000), and it has been used to administer plasmid DNA intrathecally to improve transgene expression over naked plasma (Shi et al., 2003). Since the molecular weight of PEG is easily controlled, and it is easily grafted to other molecules, specifically-sized therapies could be designed to limit drug exposure or target transfection of populations of cells most affected by the trauma. By addressing BSCB damage as early as possible, these therapies could reduce the severity of secondary damage to the spinal cord, though the designed therapy could be modified to reflect delivery through the BSCB that has been additionally compromised by secondary insults.

The formation of a necrotic, cystic cavity is common following injury and is related to the initial mechanical insult and progressive damage from secondary effects, such as ischemia (Mautes et al., 2000). At the epicenter of injury, the cystic cavity usually includes the gray matter and part of the white matter (Noble and Wrathall, 1985). Though we studied immediate, mechanical trauma to the microvasculature and thus did not allow for tissue necrosis before sacrifice, the general patterns of immediate extravasation are consistent with the profile of the cystic cavity. This is consistent with previous observations that the cystic cavity is similar in size and shape to early hemorrhage (Noble and Wrathall, 1989a,b), but also suggests that sub-hemorrhagic mechanical damage may be linked to cavity formation.

This study also demonstrates that, potentially, by applying an appropriate amount of stress or strain to a specific location in the spinal cord, the BSCB can become temporarily permeable up to a specific size, allowing focal delivery of therapeutic agents. This may be accomplished, for instance, by using focused ultrasound to cavitate intravascular microbubbles (nominally injected to provide contrast during ultrasound imaging) to produce very localized stress fields. This process has been employed to localize BBB disruption *in vivo*, but settings, such as bubble size, ultrasound frequency and power, are found empirically, and the damage, though very focal, can be severe, increasing permeability for at least 3 days (Unger et al., 2004). Any improvement in this methodology could have significant implications in the treatment of CNS diseases and disorders, including targeting specific regions for cancer therapeutics.

ACKNOWLEDGMENTS

The assistance of Wise Young and the personnel at the W.M. Keck Center for Collaborative Neuroscience at Rutgers University is greatly appreciated. Funding for this study was provided by the Centers for Disease Control to D.I.S. (R49CCR 221744-01) and a graduate fellowship to J.T.M. from the New Jersey Commission on Spinal Cord Research (04-2903-SCR-E-0).

REFERENCES

AMAR, A.P., and LEVY, M.L. (1999). Pathogenesis and pharmacological strategies for mitigating secondary damage in acute spinal cord injury. Neurosurgery **44,** 1027–1040.

ANDERSON, A.J., ROBERT, S., HUANG, W., YOUNG, W., and COTMAN, C. W. (2004). Activation of complement pathways after contusion-induced spinal cord injury. J. Neurotrauma **21,** 1831–1846.

ARBOGAST, K.B., and MARGULIES, S.S. (1998). Material characterization of the brainstem from oscillatory shear tests. J. Biomech. **31,** 801–807.

BALENTINE, J.D. (1978). Pathology of experimental spinal cord trauma. I. The necrotic lesion as a function of vascular injury. Lab. Invest. **39,** 236–253.

BAO, F., DEKABAN, G.A., and WEAVER, L.C. (2005). Anti-CD11d antibody treatment reduces free radical formation and cell death in the injured spinal cord of rats. J. Neurochem. **94,** 1361–1373.

BAPTISTE, D.C., and FEHLINGS, M.G. (2006). Pharmacological approaches to repair the injured spinal cord. J. Neurotrauma **23,** 318–334.

BASSO, D.M., BEATTIE, M.S., and BRESNAHAN, J.C. (1996). Graded histological and locomotor outcomes after spinal cord contusion using the NYU weight-drop device versus transection. Exp. Neurol. **139,** 244–256.

BEGGS, J.L., and WAGGENER, J.D. (1975). Vasogenic edema in the injured spinal cord: a method of evaluating the extent of blood–brain barrier alteration to horseradish peroxidase. Exp. Neurol. **49,** 86–96.

BEGGS, J.L., and WAGGENER, J.D. (1976). Transendothelial vesicular transport of protein following compression injury to the spinal cord. Lab. Invest. **34,** 428–439.

BERKOWITZ, E.D. (1998). Revealing America's welfare state. [Review of: Howard, C., The hidden welfare state: tax expenditures and social policy in the United States. Princeton University Press, 1997]. Rev. Am. Hist. **26,** 620–624.

BILGEN, M., and NARAYANA, P.A. (2001). A pharmacokinetic model for quantitative evaluation of spinal cord injury with dynamic contrast-enhanced magnetic resonance imaging. Magn. Reson. Med. **46,** 1099–1106.

BILSTON, L.E., LIU, Z., and PHAN-THIEN, N. (2001). Large strain behaviour of brain tissue in shear: some experimental data and differential constitutive model. Biorheology **38,** 335–345.

BLIGHT, A.R. (1992). Macrophages and inflammatory damage in spinal cord injury. J. Neurotrauma **9,** Suppl 1, S83–S91.

BORGENS, R.B., and SHI, R. (2000). Immediate recovery from spinal cord injury through molecular repair of nerve membranes with polyethylene glycol. FASEB J. **14,** 27–35.

BOTTI, R.E., TRISCARI, J., PAN, H.Y., and ZAYAT, J. (1991). Concentrations of pravastatin and lovastatin in cerebrospinal fluid in healthy subjects. Clin. Neuropharmacol. **14,** 256–261.

BRESNAHAN, J.C., BEATTIE, M.S., TODD, F.D., 3RD, and NOYES, D.H. (1987). A behavioral and anatomical analysis of spinal cord injury produced by a feedback-controlled impaction device. Exp. Neurol. **95,** 548–570.

DEMJEN, D., KLUSSMANN, S., KLEBER, S., et al. (2004). Neutralization of CD95 ligand promotes regeneration and functional recovery after spinal cord injury. Nat. Med. **10,** 389–395.

DOHRMANN, G.J., PANJABI, M.M., and WAGNER, F.C., JR. (1976). An apparatus for quantitating experimental spinal cord trauma. Surg. Neurol. **5,** 315–318.

DOHRMANN, G.J., and WICK, K.M. (1971). Demonstration of the microvasculature of the spinal cord by intravenous injection of the fluorescent dye, thioflavine S. Stain Technol. **46,** 321–322.

FADEN, A.I., GANNON, A., and BASBAUM, A.I. (1988). Use of serotonin immunocytochemistry as a marker of injury severity after experimental spinal trauma in rats. Brain Res. **450,** 94–100.

FAROOQUE, M., ZHANG, Y., HOLTZ, A., and OLSSON, Y. (1992). Exudation of fibronectin and albumin after spinal cord injury in rats. Acta Neuropathol. (Berl.) **84,** 613–620.

FEHLINGS, M.G., and TATOR, C.H. (1995). The relationships among the severity of spinal cord injury, residual neurological function, axon counts, and counts of retrogradely labeled neurons after experimental spinal cord injury. Exp. Neurol. **132,** 220–228.

GRIFFITHS, I.R., and MILLER, R. (1974). Vascular permeability to protein and vasogenic oedema in experimental concussive injuries to the canine spinal cord. J. Neurol. Sci. **22,** 291–304.

HERNANDEZ, L.A., GRISHAM, M.B., TWOHIG, B., ARFORS, K.E., HARLAN, J.M. and GRANGER, D.N. (1987). Role of neutrophils in ischemia-reperfusion-induced microvascular injury. Am. J. Physiol. **253,** H699–H703.

JAEGER, C.B., and BLIGHT, A.R. (1997). Spinal cord compression injury in guinea pigs: structural changes of endothelium and its perivascular cell associations after blood-brain barrier breakdown and repair. Exp. Neurol. **144,** 381–399.

MAUTES, A.E., WEINZIERL, M.R., DONOVAN, F., and NOBLE, L.J. (2000). Vascular events after spinal cord injury: contribution to secondary pathogenesis. Phys. Ther. **80,** 673–687.

McKENZIE, A.L., HALL, J.J., AIHARA, N., FUKUDA, K., and NOBLE, L.J. (1995). Immunolocalization of endothelin in the traumatized spinal cord: relationship to blood–spinal cord barrier breakdown. J. Neurotrauma **12,** 257–268.

MOORADIAN, A.D., HAAS, M.J., BATEJKO, O., HOVSEPYAN, M., and FEMAN, S. S. (2005). Statins ameliorate endothelial barrier permeability changes in the cerebral tissue of streptozotocin-induced diabetic rats. Diabetes **54,** 2977–2982.

NOBLE, L.J., MAUTES, A.E., and HALL, J.J. (1996). Characterization of the microvascular glycocalyx in normal and injured spinal cord in the rat. J. Comp. Neurol. **376,** 542–556.

NOBLE, L.J., and MAXWELL, D.S. (1983). Blood–spinal cord barrier response to transection. Exp. Neurol. **79,** 188–199.

NOBLE, L.J., and WRATHALL, J.R. (1985). Spinal cord contusion in the rat: morphometric analyses of alterations in the spinal cord. Exp. Neurol. **88,** 135–149.

NOBLE, L.J., and WRATHALL, J.R. (1987). The blood–spinal cord barrier after injury: pattern of vascular events proximal and distal to a transection in the rat. Brain Res. **424,** 177–188.

NOBLE, L.J., and WRATHALL, J.R. (1989a). Correlative analyses of lesion development and functional status after graded spinal cord contusive injuries in the rat. Exp. Neurol. **103,** 34–40.

NOBLE, L.J., and WRATHALL, J.R. (1989b). Distribution and time course of protein extravasation in the rat spinal cord after contusive injury. Brain Res. **482,** 57–66.

NOYES, D.H. (1987). Electromechanical impactor for producing experimental spinal cord injury in animals. Med. Biol. Eng. Comput. **25,** 335–340.

PAN, W., BANKS, W.A., and KASTIN, A.J. (1997). Blood–brain barrier permeability to ebiratide and TNF in acute spinal cord injury. Exp. Neurol. **146,** 367–373.

PAN, W., ZHANG, L., LIAO, J., CSERNUS, B., and KASTIN, A.J. (2003). Selective increase in TNF alpha permeation across the blood–spinal cord barrier after SCI. J. Neuroimmunol. **134,** 111–117.

PANNU, R., BARBOSA, E., SINGH, A.K., and SINGH, I. (2005). Attenuation of acute inflammatory response by atorvastatin after spinal cord injury in rats. J. Neurosci. Res. **79,** 340–350.

POPOVICH, P.G., HORNER, P.J., MULLIN, B.B., and STOKES, B.T. (1996). A quantitative spatial analysis of the blood–spinal cord barrier. I. Permeability changes after experimental spinal contusion injury. Exp. Neurol. **142,** 258–275.

POPOVICH, P.G., REINHARD, J.F., JR., FLANAGAN, E.M., and STOKES, B.T. (1994). Elevation of the neurotoxin quinolinic acid occurs following spinal cord trauma. Brain Res. **633,** 348–352.

POPOVICH, P.G., WEI, P., and STOKES, B.T. (1997). Cellular inflammatory response after spinal cord injury in Sprague-Dawley and Lewis rats. J. Comp. Neurol. **377,** 443–464.

PRANGE, M.T., and MARGULIES, S.S. (2002). Regional, directional, and age-dependent properties of the brain undergoing large deformation. J. Biomech. Eng. **124,** 244–252.

SAVILLE, L.R., POSPISIL, C.H., MAWHINNEY, L.A., et al. (2004). A monoclonal antibody to CD11d reduces the inflammatory infiltrate into the injured spinal cord: a potential neuroprotective treatment. J. Neuroimmunol. **156,** 42–57.

SHARMA, H.S. (2005). Pathophysiology of blood–spinal cord barrier in traumatic injury and repair. Curr. Pharm. Des. **11,** 1353–1389.

SHI, L., TANG, G.P., GAO, S.J., et al. (2003). Repeated intrathecal administration of plasmid DNA complexed with polyethylene glycol-grafted polyethylenimine led to prolonged transgene expression in the spinal cord. Gene Ther. **10,** 1179–1188.

SPARKS, D.L., CONNOR, D.J., BROWNE, P.J., LOPEZ, J.E., and SABBAGH, M.N. (2002). HMG-CoA reductase inhibitors (statins) in the treatment of Alzheimer's disease and why it would be ill-advise to use one that crosses the blood–brain barrier. J. Nutr. Health Aging **6,** 324–331.

STANISLAUS, R., PAHAN, K., SINGH, A.K., and SINGH, I. (1999). Amelioration of experimental allergic encephalomyelitis in Lewis rats by lovastatin. Neurosci. Lett. **269,** 71–74.

STANISLAUS, R., SINGH, A.K., and SINGH, I. (2001). Lovastatin treatment decreases mononuclear cell infiltration into the CNS of Lewis rats with experimental allergic encephalomyelitis. J. Neurosci. Res. **66,** 155–162.

STEWART, W.W. (1981). Lucifer dyes—highly fluorescent dyes for biological tracing. Nature **292,** 17–21.

STOKES, B.T., NOYES, D.H., and BEHRMANN, D.L. (1992). An electromechanical spinal injury technique with dynamic sensitivity. J. Neurotrauma **9,** 187–195.

SUGIO, S., KASHIMA, A., MOCHIZUKI, S., NODA, M., and KOBAYASHI, K. (1999). Crystal structure of human serum albumin at 2.5 A resolution. Protein Eng. **12,** 439–446.

TERAE, S., TAKAHASHI, C., ABE, S., KIKUCHI, Y., and MIYASAKA, K. (1997). Gd-DTPA-enhanced MR imaging of injured spinal cord. Clin. Imaging **21,** 82–89.

UNGER, E.C., PORTER, T., CULP, W., LABELL, R., MATSUNAGA, T., and ZUTSHI, R. (2004). Therapeutic applications of lipid-coated microbubbles. Adv. Drug Deliv. Rev. **56,** 1291–1314.

WAGNER, F.C., JR., and STEWART, W.B. (1981). Effect of trauma dose on spinal cord edema. J. Neurosurg. **54,** 802–806.

WESTMARK, R., NOBLE, L.J., FUKUDA, K., AIHARA, N., and McKENZIE, A.L. (1995). Intrathecal administration of endothelin-1 in the rat: impact on spinal cord blood flow and the blood–spinal cord barrier. Neurosci. Lett. **192,** 173–176.

WHETSTONE, W.D., HSU, J.Y., EISENBERG, M., WERB, Z., and NOBLE-HAEUSSLEIN, L.J. (2003). Blood–spinal cord barrier after spinal cord injury: relation to revascularization and wound healing. J. Neurosci. Res. **74,** 227–239.

YOUNG, W. (2002). Spinal cord contusion models. Prog. Brain Res. **137,** 231–255.

Address reprint requests to:
David I. Shreiber, Ph.D.
Department of Biomedical Engineering
Rutgers, The State University
599 Taylor Road
Piscataway, NJ 08854

E-mail: shreiber@rci.rutgers.edu